Nematic fluctuations and phase transitions in LaFeAsO: A Raman scattering study

U. F. Kaneko, P. F. Gomes, A. F. García-Flores, J.-Q. Yan, T. A. Lograsso, G. E. Barberis, D. Vaknin, and E. Granado

Phys. Rev. B **96**, 014506 — Published 10 July 2017

DOI: 10.1103/PhysRevB.96.014506

Nematic Fluctuations and Phase Transitions in LaFeAsO: a Raman Scattering Study

U. F. Kaneko,[1] P. F. Gomes,[1,2] A. F. García-Flores,[3] J.-Q. Yan*,[4]
T. A. Lograsso,[4,5] G. E. Barberis,[1] D. Vaknin,[4,6] and E. Granado[1]

[1] *"Gleb Wataghin" Institute of Physics, University of Campinas - UNICAMP, Campinas, São Paulo 13083-859, Brazil*
[2] *Federal University of Goiás - UFG, Jataí, Goiás 75801-615, Brazil*
[3] *Federal University of ABC - UFABC, Santo André, São Paulo 09210-580, Brazil*
[4] *Ames Laboratory, US-DOE, Ames, Iowa 50011, USA*
[5] *Department of Materials Sciences and Engineering, Iowa State University, Ames, Iowa 50011, USA.*
[6] *Department of Physics and Astronomy, Iowa State University, Ames, Iowa 50011, USA*

Raman scattering experiments on LaFeAsO with distinct antiferromagnetic (T_{AFM} = 140 K) and tetragonal-orthorhombic (T_S = 155 K) transitions show a quasi-elastic peak (QEP) in B_{2g} symmetry (2 Fe tetragonal cell) that fades away below $\sim T_{AFM}$ and is ascribed to electronic nematic fluctuations. A scaling of the reported shear modulus with the $T-$dependence of the QEP height rather than the QEP area indicates that magnetic degrees of freedom drive the structural transition. The large separation between T_S and T_{AFM} in LaFeAsO compared to $BaFe_2As_2$ manifests itself in slower dynamics of nematic fluctuations in the former.

PACS numbers: 74.70.Xa, 74.25.nd

The discovery of Fe-based superconductors (FeSCs) with high transition temperatures (above 100 K in FeSe films[1]) triggered much interest on these materials.[2–5] Nematicity, characterized by large in-plane electronic transport anisotropy,[6,7] is normally observed below a tetragonal-orthorhombic transition temperature T_S, and seems to be also present in other high-T_c superconductors.[8] Also, divergent nematic susceptibility in the optimal doping regime suggests that nematic fluctuations play an important role in the superconducting pairing mechanism.[9] Thus, investigations of the nematic order and fluctuations in FeSCs and their parent materials are pivotal to unraveling the origin of high-T_c superconductivity. Clearly, it is necessary to identify the primary order parameter associated with the nematic phase.[4,5] A relation between nematicity and magnetism is suggested by the near coincidence between T_S and the antiferromagnetic (AFM) ordering temperature T_{AFM} in some materials, most notably $BaFe_2As_2$ with $T_{AFM} \sim T_S = 138$ K.[10,11] In fact, the magnetic ground state is a stripe AFM phase that breaks the 4-fold tetragonal symmetry of the lattice (see Fig. 1(a)), providing a natural mechanism for electronic anisotropy. On the other hand, T_S and T_{AFM} are significantly separated for LaFeAsO (LFAO) (T_{AFM} = 140 K and T_S = 155 K),[7,12–14] while FeSe does not order magnetically at ambient pressure but still shows a nematic transition at T_S = 90 K,[15] motivating suggestions that the nematic transition may be driven by charge/orbital degrees of freedom rather than magnetism in the latter.[17,18] However, even for FeSe the magnetic scenario may still apply.[19] In $Ba(Fe_{1-x}Co_x)_2As_2$ and other doped systems, the splitting between T_{AFM} and T_S increases with doping.[10,16] Overall, the primary order parameter that drives the structural/nematic transition at T_S and the dominating mechanism of T_{AFM}/T_S separation in parent FeSCs are not fully settled yet.

Raman scattering was recently employed as a probe of nematic fluctuations in FeSCs and their parent materials. In $A(Fe_{1-x}Co_x)_2As_2$ (A = Ca, Sr, Ba, Eu)[20–26], $Ba_{1-p}K_pFe_2As_2$,[26] FeSe[27,28] and $NaFe_{1-x}Co_xAs$,[29] a quasi-elastic peak (QEP) with B_{2g} symmetry (considering the 2 Fe tetragonal cell, see Fig. 1(a)) has been observed and interpreted in terms of either charge/orbital[22,23,25,27,30] or spin[24,26,31–33] nematic fluctuations. An unambiguous experimental identification of the nature of the fluctuations generating the B_{2g} Raman QEP (charge/orbital or magnetic) is challenging due to the inherent coupling between the corresponding degrees of freedom. Despite such extensive investigations in several materials, no Raman study of the nematic fluctuations in the key parent compound LFAO has been carried out yet. In this work, we fill this gap and investigate in detail the temperature dependence of both electronic and phonon Raman scattering in LFAO.

Details of the synthesis procedure and basic characterization of the crystal employed in this work, showing T_S = 155 K and T_{AFM} = 140 K, are described elsewhere.[13,34] A fresh ab surface with $\sim 1 \times 1$ mm^2 was obtained by cleaving the crystal and immediately mounting it at the cold finger of a closed-cycle He cryostat. The polarized Raman spectra were taken in quasi-backscattering geometry using the 488.0 nm line as exciting source focused into the ab surface with a spot of ~ 50 μm diameter. A triple 1800 mm^{-1} grating spectrometer equipped with a LN_2-cooled multichannel CCD detector was employed. The instrumental linewidth was ~ 4 cm^{-1}. Figure 1(a) illustrates a square lattice of the Fe atoms and sets the conventions for polarizations. The 2 Fe tetragonal (space group P4/mmm) and 4 Fe or-

*Present address: Materials Science and Technology Division, Oak Ridge National Laboratory, Oak Ridge, Tennessee 37831, USA.

thorhombic (space group Cmma) unit cells and axes in the ab plane are also represented.

Symmetry analysis indicates that four Raman-active phonons are accessible by our experimental geometry in both tetragonal ($2A_{1g}$ and $2B_{1g}$) and orthorhombic ($2A_g$ and $2B_{1g}$) phases. Illustrations of such modes are given in Fig. 1(b) (see also Ref.[35]). The raw Raman spectra in the phonon region at distinct linear polarizations are given in Figs. 1(c) (T = 20 K) and 1(d) (T = 290 K). The B_{1g} modes observed at 203 and 317 cm^{-1} at T = 290 K are ascribed to Fe and O vibrations along c, respectively,[35] while the A_{1g} modes at 164 and 208 cm^{-1} are ascribed to As and La vibrations along c. The position of the 164 cm^{-1} mode is comparable to that reported for the As mode in NaFeAs (163 cm^{-1})[36] and in AFe$_2$As$_2$ (A = Ca, Sr, Ba) (180-190 cm^{-1}).[21,37–39] The T-dependence of this phonon was investigated in detail [see Supplemental Material (SM)[40]]. Its linewidth at low-T is resolution-limited, suggesting a high crystalline quality, and shows a maximum at $T \sim T_{AFM}$ with no anomaly at T_S. Frequency anomalies are observed for this mode at both T_S and T_{AFM}. Finally, an enhancement in XY polarization is observed below T_{AFM}, which is similar to related systems[21,24,37,39] and is due to the coupling of this phonon with anisotropic electronic states in the magnetic phase.[41]

The Raman response $\chi''(\omega,T)$ is related to the raw intensity I through the relation $I = (1+n)\chi''(\omega,T) + D$, where $n \equiv 1/(e^{\hbar\omega/k_BT}-1)$ is the Bose-Einstein statistical factor and D is an intensity offset (for details, see SM[40]). Figures 2(a-e) show $\chi''(\omega,T)$ in XY polarization corresponding to B_{2g} symmetry in the 2 Fe tetragonal cell. These measurements were made with much less laser power ($\sim$ 3 mW) than for the data shown in Fig. 1 ($\sim$ 10 mW), in order to minimize laser heating effects,[24] and were also taken with 4× less exposure times due to the large number of investigated temperatures. These limitations resulted in poorer signal-to-noise in the data shown in Figs. 2(a-e). An 8-point-average smoothing is applied in these data for better visualization of the broad electronic Raman signal. $\chi''(\omega,T)$ data with better statistics at selected temperatures are also presented in the SM.[40] A linear component for $\chi''_{B_{2g}}(\omega,T)$ is observed in the frequency region below 600 cm^{-1}, which is enhanced below T_{AFM}. Measurements performed on an extended frequency region show this component is part of broad peaks at $\sim 2400-3000$ cm^{-1} (see SM[40]). A similar structure was found in BaFe$_2$As$_2$ and attributed to two-magnon scattering.[42] An additional scattering channel, which is most evident at low frequencies ($\omega \lesssim 150$ cm^{-1}), is observed in this symmetry and enhances on cooling down to $\sim$ 140 K, fading away on further cooling. This contribution is satisfactorily fitted by a quasi-elastic peak (QEP) $(\chi'')^{B_{2g}}_{QEP}(\omega,T) = A(T)\omega\Gamma(T)/(\omega^2+\Gamma(T)^2)$ (dashed lines in Figs. 2(a-d)), corresponding to a Lorentzian lineshape for $(\chi'')^{B_{2g}}_{QEP}(\omega,T)/\omega$. It can be seen from Fig. 2(f) that the relatively large noise in the Raman response

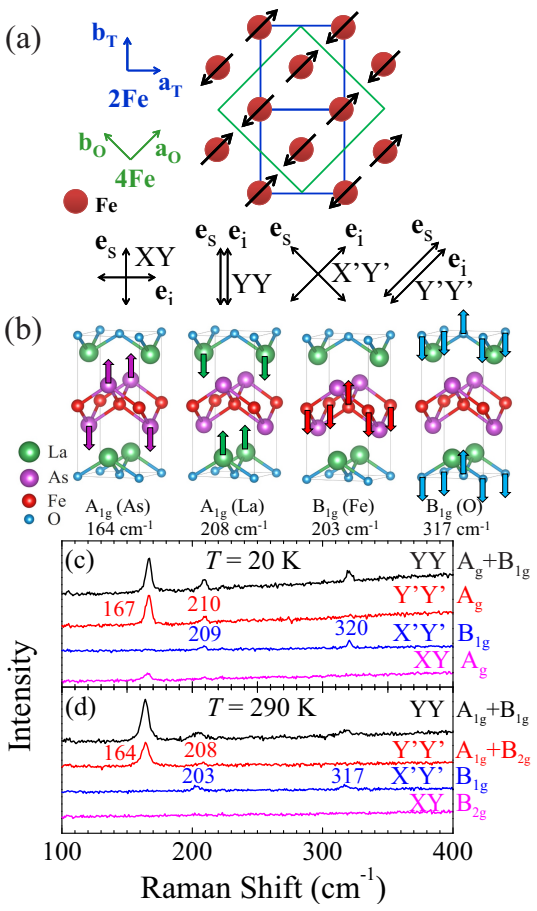

FIG. 1: (Color online) (a) Schematic view of the Fe square lattice with the stripe antiferromagnetic structure and representations of the XY, YY, $X'Y'$ and $Y'Y'$ linear polarizations. The unit vectors $\mathbf{e}_i$ and $\mathbf{e}_s$ represent the polarizations of the incident and scattered photons, respectively. The edges and axes for the 2 Fe tetragonal and 4 Fe orthorhombic unit cells are also displayed; (b) Raman-active phonons accessible in the scattering geometry employed in this work. The corresponding symmetries and observed frequencies at 290 K are indicated; (c,d) Raman spectra for distinct polarizations at T = 20 K (c) and T = 290 K (d). In (c) and (d), the symmetry associated with each polarization is given with respect to the corresponding orthorhombic and tetragonal unit cells.

above $\sim$ 150 cm^{-1} have little influence on the determination of the QEP fitting parameters $A(T)$ and $\Gamma(T)$. The Raman response (χ'') for other symmetries accessible by our experimental setup are given in SM at selected temperatures.[40]

Figures 3(a) and 3(b) show the T-dependence of the Lorentzian B_{2g} QEP area A and width Γ, respectively. Only data between $\sim$ 120 and 200 K are shown, corresponding to the $T-$interval where this signal is sufficiently strong to warrant reliable Lorentzian fits within our statistics. Figure 3(c) shows A/Γ, corresponding to the QEP height, while Fig. 3(d) is a zoom in of Fig. 3(b) near T_S. Between 280 and 120 K, the B_{2g} QEP area and height show a maximum at T_{max} = 143 K, slightly

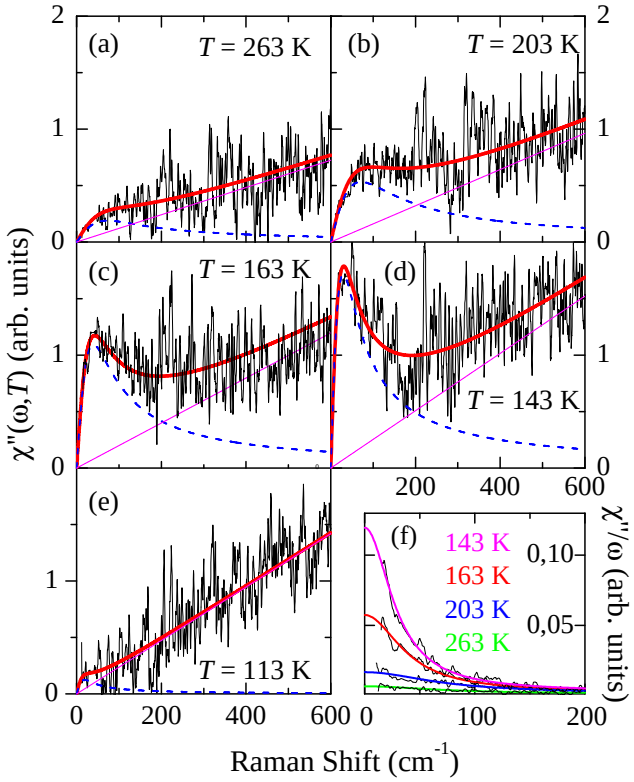

FIG. 2: (Color online) (a-e) Raman response $\chi''(\omega, T)$ in B_{2g} symmetry for the tetragonal cell (XY polarization) at selected temperatures. The thick lines are fittings to a model including a Lorentzian quasi-elastic peak (QEP, dashed line) and an additional linear contribution (thin solid line) (see text). (f) $\chi''(\omega, T)/\omega$ at selected temperatures and corresponding fits to the QEP model.

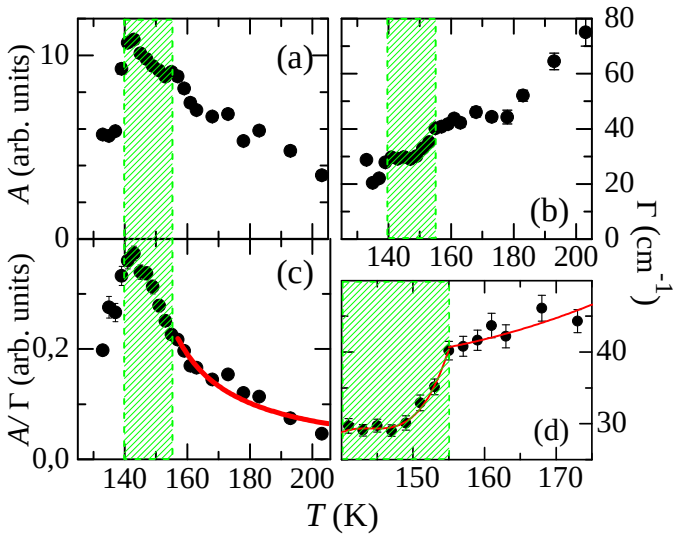

FIG. 3: (Color online) T-dependence of (a) area A, (b,d) width Γ and (c) height A/Γ of B_{2g} Lorentzian QEP (2 Fe tetragonal cell). Error bars, when not displayed, are smaller than the symbol sizes. The shaded areas mark the $T_{AFM} < T < T_S$ interval. The solid line in (c) shows a fit of the B_{2g} QEP height to a Curie-Weiss-like behavior between T_S and ~ 200 K, yielding $\theta_{CW} = 137(3)$ K (see text). The solid line in (d) is a guide to the eyes.

above T_{AFM}, nearly vanishing below 120 K. Concerning the widths, the B_{2g} QEP gradually sharpens on cooling down to T_S. Below T_S, Γ_{QEP} further sharpens from ~ 40 to ~ 30 cm^{-1}.

As for the other FeSCs,[22–27,30,32,33] we ascribe the B_{2g} QEP in LFAO to electronic nematic fluctuations. The significant residual nematic fluctuations observed between ~ 120 K and T_{AFM} (see Figs. 3(a,c)) are consistent with ^{75}As NMR measurements that show coexisting AFM and paramagnetic regions in this T-interval;[43] the paramagnetic regions are expected to host the residual nematic fluctuations observed here. Intriguingly, the temperature where the QEP area and height are maxima, T_{max}, does not coincide with the bulk-average T_S, contrary to other parent FeSCs.[24,27] This deviation is likely related to the broad T interval where tetragonal and orthorhombic domains coexist and fluctuate.[44] In this scenario, while the QEP intensity per orthorhombic unit volume is expected to be reduced on cooling, the inverse

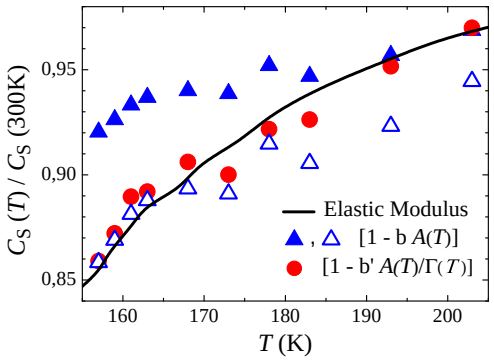

FIG. 4: (Color online) Temperature dependence of the polycrystalline shear modulus taken from Ref.[12] (solid line), and attempted scalings of this curve to the B_{2g} QEP Area $A(T)$ (open and solid triangles) and height $A(T)/\Gamma(T)$ (circles) extracted from Figs. 3(a) and 3(c), respectively.

tendency is found for the remaining tetragonal domains, leading to $T_{max} < T_S$. Still, the nematic fluctuations in LFAO are clearly sensitive to T_S, as demonstrated by the sharpening of the B_{2g} QEP below T_S (see Fig. 3(d)). In fact, this is a manifestation of slower nematic fluctuations in the orthorhombic phase. This is again qualitatively consistent with ^{75}As NMR results that show a slowing down of the magnetic dynamics below T_S[43] and may be also related with the enhancement of the magnetic cor-

relation length below T_S observed in inelastic neutron scattering measurements.[34]

Although both spin and orbital/charge nematic fluctuations are arguably present in LFAO and coupled to each other, the Raman activity of magnetic and charge fluctuations arises from entirely different mechanisms,[23,31] and most likely the Raman intensities will be dominated by one of them. We discuss our results considering separately the independent scenarios where charge/orbital or spin nematic fluctuations dominate the intensity of the B_{2g} Raman QEP. Starting with the charge/orbital scenario (scenario A), the bare static nematic susceptibility $\chi^{(0)}_{nem}(T)$ and $(\chi^{''})^{B_{2g}}_{QEP}(\omega,T)$ are directly connected by a Kramers-Kronig transformation $\chi^{(0)}_{nem}(T) = (2/\pi)\int_0^\infty (\chi^{''})^{B_{2g}}_{QEP}(\omega,T)/\omega d\omega$,[22,23] corresponding to the QEP area $A(T)$ in our analysis. An attempted scaling of $\chi^{(0)}_{nem}(T)$ obtained in this way and the polycrystalline shear modulus C_S extracted from Ref.[12], i.e., $C_S(T)/C_S(300\text{ K}) = 1 - bA(T)$ (Ref.[23]) is given in Fig. 4, where b is a free parameter (see footnote[45]). In our analysis, we tentatively varied b to scale $A(T)$ to $C_S(T)$ either at $T \gtrsim T_S$ (empty triangles in Fig. 4) or at $T \sim 200$ K $>> T_S$ (filled triangles). However, no value for b yielded a satisfactory scaling for the entire investigated interval $T_S < T \lesssim 200$ K. The lack of scaling between the shear modulus and the QEP area, interpreted under scenario A, indicate that the charge/orbital fluctuations do not drive the structural transition at T_S, and an additional electronic nematic degree of freedom, presumably the magnetic one, is driving the phase transitions in LFAO.[5] This reasoning closely follows that presented in Ref.[22] for $BaFe_2As_2$.

We now explore the alternative scenario where spin nematic fluctuations dominate the intensity of the B_{2g} Raman QEP (scenario B). In this case, the dynamical electronic nematic susceptibility is not given directly by $(\chi^{''})^{B_{2g}}_{QEP}(\omega,T)$, and therefore a Kramers-Kronig transformation does not apply to extract $\chi^{(0)}_{nem}(T)$. Instead, $\chi^{(0)}_{nem}(T)$ is proportional to the slope of $(\chi^{''})^{B_{2g}}_{QEP}(\omega,T)$ in the limit $\omega \to 0$,[24,31] namely the QEP height $A(T)/\Gamma(T)$. In this scenario, $\Theta_{in} = 137(3)$ K, obtained from the fit of $A(T)/\Gamma(T)$ to a Curie-Weiss-like behavior $A/\Gamma = C/(T-\Theta_{in})$ over the interval $T_S < T \lesssim 200$ K (solid line in Fig. 3(c)), is the bare nematic transition temperature in the absence of the magneto-elastic coupling that induces the transition at higher temperatures. Figure 4 displays a scaling of the polycrystalline shear modulus to the peak height, $C_S(T)/C_S(300\text{ K}) = 1 - b'A(T)/\Gamma(T)$, showing an excellent agreement for the entire investigated interval. Therefore, independently of the assumption on the detailed nature of the Raman B_{2g} QEP, our analysis supports the scenario where the nematic transition is magnetically driven.

The thermal evolution of the relaxation rate $\Gamma^{B_{2g}}$ provides further insight into the nematic transition. At $T \sim 200$ K one has $\Gamma^{B_{2g}} \sim 10$ meV (~ 80 cm^{-1}), see Fig. 3(b), which is on the same energy scale of the optical phonons (see Fig. 1). However, the nematic fluctuations slow down continuously on cooling (see Fig. 3(b)). Presumably, as the nematic fluctuation rate become significantly smaller than the typical optical phonon frequencies, local and instantaneous orthorhombic distortions are expected to rise and accompany the electronic nematic correlations, as the nuclei positions will have sufficient time to respond to the electronic nematic fluctuations. We suggest that at T_S the growing lattice strain caused by the local orthorhombic distortions finally drive the formation of a long-range orthorhombic phase, i.e., the so-called nematic phase. Immediately below T_S the nematic fluctuations are slowed down further (see Fig. 3(d)). This is likely associated with changes in the J_a and J_b nearest-neighbor exchange integrals, partially releasing the magnetic frustration and allowing for increased magnetic correlation lengths.[34]

Further inspection of our results gives insight into the large separation between T_S and T_{AFM} (15 K) compared to their near coincidence in $BaFe_2As_2$. We note that at $T = 163$ K, for instance, the maximum of $\chi^{''}_{B_{2g}}(\omega,T)$, corresponding to the QEP linewidth Γ, is 43(2) cm^{-1} for LFAO (see Fig. 2(c) and 3(d)), much smaller than ~ 100 cm^{-1} for BFA at this temperature.[22] Such slower nematic fluctuations in LFAO preempt the stabilization of orthorhombic domains significantly above T_{AFM}. This scenario may also give insight into the nematic transition of other FeSCs. For instance, a B_{2g} QEP has also been reported for FeSe,[27] which also gradually sharpens on cooling, reaching $\Gamma \sim 30$ cm^{-1} at T_S, which is comparable to the observed Γ for LFAO in the nematic phase (see Fig. 3(d)).

In summary, polarized Raman scattering in LaFeAsO reveals a quasi-elastic B_{2g} scattering channel from nematic fluctuations above $\sim T_{AFM}$. An analysis of the T-dependence of this signal supports the conclusion that spin degrees of freedom are the primary driver of the phase transitions in this material. Relatively slow electronic nematic fluctuations preempt T_S and arguably signal the large separation between T_S and T_{AFM}.

We thank R. M. Fernandes and P. G. Pagliuso for their critical reading of this manuscript and helpful discussions. This work was supported by FAPESP Grant 2012/04870-7 and CNPq, Brazil. Ames Laboratory is supported by the US Department of Energy, Office of Basic Energy Sciences, Division of Materials Sciences and Engineering under Contract No. DE-AC02-07CH11358.

[1] J.-F. Ge, Z.-L. Liu, C. Liu, C.-L. Gao, D. Qian, Q.-K. Xue, Y. Liu and J.-F. Jia, Nature Mater. **14**, 285 (2015).

[2] Kamihara, T. Watanabe, M. Hirano, and H. Hosono, J.

Am. Chem. Soc. **130**, 3296 (2008).
[3] J. Paglione and R.L. Greene, Nature Phys. **6** 645 (2010).
[4] R.M. Fernandes and J. Schmalian, Supercond. Sci. Technol. **25**, 084005 (2012).
[5] R.M. Fernandes, A.V. Chubukov, and J. Schmalian, Nature Phys. **10**, 97 (2014).
[6] J.-H. Chu, J.G. Analytis, K. De Greeve, P.L. McMahon, Z. Islam, Y. Yamamoto, and I.R. Fisher, Science **329**, 824 (2010).
[7] A. Jesche, F. Nitsche, S. Probst, Th. Doert, P. Müller, and M. Ruck, Phys. Rev. B **86**, 134511 (2012).
[8] Y. Ando, K. Segawa, S. Komiya, and A.N. Lavrov, Phys. Rev. Lett. **88**, 137005 (2002).
[9] H.-H. Kuo, J.-H. Chu, J.C. Palmstrom, S.A. Kivelson, and I.R. Fisher, Science **352**, 958 (2016).
[10] M.G. Kim, R.M. Fernandes, A. Kreyssig, J.W. kim, A. Thaler, S.L. Bud'ko, P.C. Canfield, R.J. McQueeney, J. Schmalian, and A.I. Goldman, Phys. Rev. B **83**, 134522 (2011).
[11] T.M. Garitezi, C. Adriano, P.F.S. Rosa, E.M. Bittar, L. Bufaical, R.L. de Almeida, E. Granado, T. Grant, Z. Fisk, M.A. Avila, R.A. Ribeiro, P.L. Kuhns, A.P. Reyes, R.R. Urbano, and P.G. Pagliuso, Braz. J. Phys. **43**, 223 (2013).
[12] M.A. McGuire, A.D. Christianson, A.S. Sefat, B.C. Sales, M.D. Lumsden, R. Jin E.A. Payzant, D. Mandrus, Y. Luan, V. Keppens, V. Varadarajan, J.W. Brill, R.P. Hermann, M.T. Sougrati, F. Grandjean, and G.J. Long, Phys. Rev. B **78**, 094517 (2008).
[13] J.-Q. Yan, S. Nandi, J.L. Zarestky, W. Tian, A. Kreyssig, B. Jensen, A. Kracher, K.W. Dennis, R.J. McQueeney, A.I. Goldman, R.W. McCallum, and T.A. Lograsso, Appl. Phys. Lett. **95**, 222504 (2009).
[14] H.-F. Li, W. Tian, Q.-Q. Yan, J.L. Zarestky, R.W. McCallum, T.A. Lograsso, and D. Vaknin, Phys. Rev. B **82**, 064409 (2010).
[15] T.M. McQueen, A.J. Williams, P.W. Stephens, J. Tao, Y. Zhu, V. Ksenofontov, F. Casper, C. Felser, and R.J. Cava, Phys. Rev. Lett. **103**, 057002 (2009).
[16] D.K. Pratt, W. Tian, A. Dreyssig, J.L. Zarestky, S. Nandi, N. Ni, S.L. Bud'ko, P.C. Canfield, A.I. Goldman, and R.J. McQueeney, Phys. Rev. Lett. **103**, 087001 (2009).
[17] S.-H. Baek, D.V. Efremov, J.M. Ok, J.S. Kim, J. van den Brink, and B. Büchner, Nature Mater. **14**, 210 (2014).
[18] A.E. Böhmer, T. Arai, F. Hardy, T. Hattori, T. Iye, T. Wolf, H. v. Löhneysen, K. Ishida, and C. Meingast, Phys. Rev. Lett. **114**, 027001 (2015).
[19] A.V. Chubukov, R.M. Fernandes, and J. Schmalian, Phys. Rev. B **91**, 201105(R) (2015).
[20] L. Chauvière, Y. Gallais, M. Cazayous, M.A. Méasson, A. Sacuto, D. Colson, and A. Forget Phys. Rev. B **82**, 180521(R) (2010).
[21] L. Chauvière, Y. Gallais, M. Cazayous, M.A. Méasson, A. Sacuto, D. Colson, and A. Forget, Phys. Rev. B **84**, 104508 (2011).
[22] Y. Gallais, R.M. Fernandes, I. Paul, L. Chauvière, Y.-X. Yang, M.-A. Méasson, M. Cazayous, A. Sacuto, D. Colson, and A. Forget, Phys. Rev. Lett. **111**, 267001 (2013).
[23] Y. Gallais and I. Paul, C. R. Physique **17**, 113 (2016).
[24] F. Kretzschmar, T. Böhm, U. Karahasanović, B. Muschler, A. Baum, D. Jost, J. Schmalian, S. Caprara, M. Grilli, C. Di Castro, J.G. Analytis, J.-H. Chu, I.R. Fisher, and R. Hackl, Nature Phys. **12**, 560 (2016).
[25] W.-L. Zhang, Z.P. Yin, A. Ignatov, Z. Bukowski, J. Karpinski, A.S. Sefat, H. Ding, P. Richard, and G. Blumberg, Phys. Rev. B **93**, 205106 (2016).
[26] T.Böhm, R. Hosseinian Ahangharnejhad, D. Jost, A. Baum, B. Muschler, F. Kretzschmar, P. Adelmann, T. Wolf, H.-H. Wen, J.-H. Chu, I.R. Fisher, and R. Hackl, arXiv: 1608.02772 (2016).
[27] P. Massat, D. Farina, I. Paul, S. Karlsson, P. Strobel, P. Toulemonde, M.-A. Méasson, M. Cazayous, A. Sacuto, S. Kasahara, T. Shibauchi, Y. Matsuda, and Y. Gallais, PNAS **113**, 9177 (2016).
[28] V. Gnezdilov, Y.G. Pashkevich, P. Lemmens, D. Wulferding, T. Shevtsova, A. Gusev, D. Chareev, and A. Vasiliev, Phys. Rev. B **87**, 144508 (2013).
[29] V.K. Thorsmolle, M. Khodas, Z.P. Yin, C. Zhang, S.V. Carr, P. Dai, and G. Blumberg, Phys. Rev. B **93**, 054515 (2016).
[30] H. Yamase and R. Zeyler, Phys. Rev. B **88**, 125120 (2013).
[31] U. Karahasanovic, F. Kretzschmar, T. Böhm, R. Hackl, I. Paul, Y. Gallais, and J. Schmalian, Phys. Rev. B **92**, 075134 (2015).
[32] M. Khodas and A. Levchenko, Phys. Rev. B **91**, 235119 (2015).
[33] H. Yamase and R. Zeyher, New J. Phys. **17**, 073030 (2015).
[34] Q. Zhang, R.M. Fernandes, J. Lamsal, J. Yan, S. Chi, G.S. Tucker, D.K. Pratt, J.W. Lynn, R.W. McCallum, P.C. Canfield, T.A. Lograsso, A.I. Goldman, D. Vaknin, and R.J. McQueeney, Phys. Rev. Lett. **114**, 057001 (2015).
[35] V.G. Hadjiev, M.N. Iliev, K. Sasmal, Y.-Y. Sun, and C.W. Chu, Phys. Rev. B **77**, 220505(R) (2008).
[36] Y.J. Um, Y. Bang, B.H. Min, Y.S. Kwon, and M. Le Tacon, Phys. Rev. B **89**, 184510 (2014).
[37] K.-Y. Choi, D. Wulferding, P. Lemmens, N. Ni, S.L. Bud'ko, and P.C. Canfield, Phys. Rev. B **78**, 212503 (2008).
[38] A.P. Litvinchuk, V.G. Hadjiev, M.N. Iliev, B. Lv, A.M. Guloy, and C.W. Chu, Phys. Rev. B **78**, 060503(R) (2008).
[39] L. Chauviére, Y. Gallais, M. Cazayous, A. Sacuto, M.A. Méasson, D. Colson, and A. Forget, Phys. Rev. B **80**, 094504 (2009).
[40] See Supplemental Material [url], which includes Ref.[47], for details on the temperature dependence of the As A_g phonon, extraction procedure of the Raman response from the raw intensities, Raman response with improved statistics at different polarizations and Raman response over an extended frequency interval.
[41] N.A. García-Martínez, B. Valenzuela, S. Ciuchi, E. Cappelluti, M.J. Calderón, and E. Bascones, Phys. Rev. B **88**, 165106 (2013).
[42] S. Sugai, Y. Mizuno, R. Watanabe, T. Kawaguchi, K. Takenaka, H. Ikuta, Y. Takayanagi, N. Hayamizu, and Y. Sone, J. Phys. Soc. Jpn. **81**, 024718 (2012).
[43] M. Fu, D.A. Torchetti, T. Imai, F.L. Ning, J.-Q. Yan, and A.S. Sefat, Phys. Rev. Lett. **109**, 247001 (2012).
[44] H.-F. Li, J.-Q. Yan, J.W. Kim, R.W. McCallum, T.A. Lograsso, and D. Vaknin, Phys. Rev. B **84**, 220501(R) (2011).
[45] There is no report on single crystal shear moduli in LFAO, to the best of our knowledge. The polycrystalline shear modulus "C_{44}" shown in ref.[12] is a superposition of the several single crystal shear moduli. However, only C_{66} is expected to become critical and display strong temperature dependence, and in our analysis we assume that it dominates the temperature-dependence of the polycrystalline shear modulus.
[46] R.M. Fernandes, L.H. VanBebber, S. Bhattacharya, P. Chandra, V. Keppens, D. Mandrus, M.A. McGuire, B.C.

Sales, A.S. Sefat, and J. Schmalian, Phys. Rev. Lett. **105**, 157003 (2010).
[47] E. Granado, A. García, J.A. Sanjurjo, C. Rettori, I. Torriani, F. Prado, R.D. Sánchez, A. Caneiro, and S.B. Oseroff, Phys. Rev. B **60**, 11879 (1999).